Supplementary material

Effect of processing conditions on the electromechanical behaviour of inkjet-printed multimaterial electronics under tensile strain

Table of Contents

Deposition strategy

Figure 1 schematically represents the printing strategy followed during the deposition on the XY plane. The blue box indicates the starting position and coverage area occupied by the printer head. The partitions (identified by the numbers) of the box represent the geometric division into pixels, and the number relates to the temporal sequence of deposition of the droplets. The dimensions of the trace exceed those of the printer head in the X and Y directions, necessitating movements along these axes to complete the printing of the specimens.

Starting from the initial position, the head jet ink opening the nozzles in the corresponding position of the #1 partition. After that, the printing plate moves along the X-axis, positioning the head above the orange box and depositing a new ink droplet in the same partition (#1). This step is repeated until the whole X dimension of the trace is fully printed. Then, the trace passes under the UV or IR lamp for curing/sintering the deposited line, depending on the material.

After that, the process is repeated for the same partition (#1) on the next column on the right (green and violet box) and so on, until the whole trace in the X is completed. The same is applied for all boxes in the Y direction. Once the trace in the X and Y direction for partition #1 is completed, the same deposition strategy is repeated for the #2 droplets and the subsequent partitions, finishing the slice with droplets #8. Subsequently, the same procedure is repeated for the next slices with a higher z coordinate.

Figure 1: printer deposition strategy

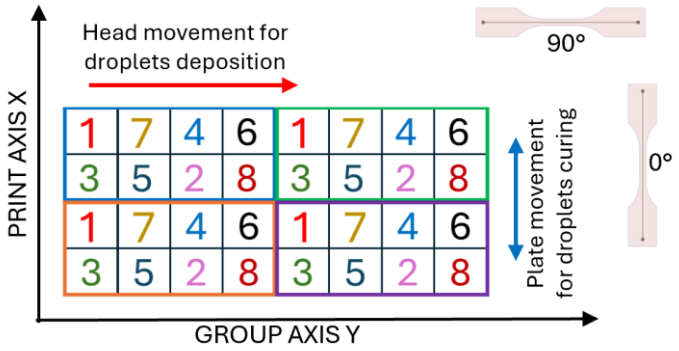

Source: figure by authors

Calibration process

The calibration process is comprised of two distinct phases. The initial phase is nozzle cancellation, wherein a controlled printing test is executed to ascertain the status of all nozzles, identifying which are operational and which are occluded. The occluded nozzles are subsequently selected and deactivated.

Following this, the second calibration step, drop volume calibration, is performed utilizing only the functional nozzles. In this phase, the volume of ejected ink is controlled by modulating the electrical voltage. The dispensed ink is then weighed, and this measurement is input into the printer. The printer subsequently employs a proprietary internal algorithm to automatically calibrate the slice thickness value.

“High quality” printing strategy defined in accordance with the machine supplier and adopted in this study to prioritise the deposition of CI droplets and then the DI one, to maximise the final conductivity. Initially, the machine deposited the CI slices according to the DI/CI thickness ratio, which ranged from 9 to 11. This parameter was automatically calculated by the printer calibration system. The dielectric was subsequently deposited as the negative counterpart of the conductive. Additionally, the high-quality strategy maximized sintering, adding a thermal cycle during the process and exposing the printing plate to the IR lamp every purge and cleaning step (every 4-5 minutes). This ensured complete solvent evaporation and sintering of the CI, reaching about 165°C.

Post-printing sintering cycle

An investigation was conducted to examine the post-printing thermal cycle to achieve complete and homogeneous Ag NP’s sintering, phenomena extensively studied in other publications regarding the 3D printing of Ag NP-based inks [1,2].

A preliminary experiment involved a post-printing thermal cycle in an oven at 200°C for 10.5 hours to achieve maximum and constant conductivity in the conductive trace. As illustrated in Figure2, the conductivity changes from $2.6*10^7$ S/mm to $2.75*10^7$ S/m, or from 41% to 43% of Ag bulk conductivity ($6.3*10^7$). It demonstrates that the "High Quality" process already ensures effective evaporation of the solvent and nearly complete sintering of Ag NPs during the printing process, renders an additional cycle in the oven unnecessary. Thermal cycle affects the mechanical properties of the dielectric part, given that the temperature exceeds Tg (145°C), and the dimension of Ag NPs. And also, as described by Zhang [3], thermal cycle at elevated temperatures increases NPs size while extending the time cycle has the opposite effect inducing a decrease in NP size, which affects the electrical properties.

Figure 2: Evolution of conductivity during the post-printing thermal cycle

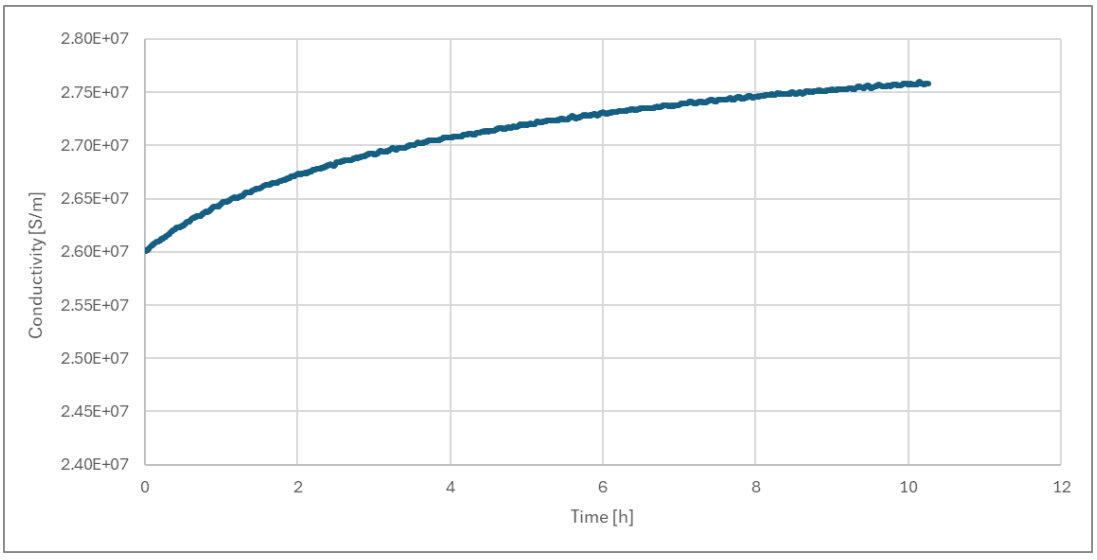

Source: figure by authors

Handling of the geometry

The slicing process was conducted using the proprietary FLIGHT™ software suite (Nano Dimension), which is specifically designed for the Dragonfly system. The software processes both three-dimensional CAD files, such as .stl or .obj, and standard two-dimensional electronic layout files, including the Gerber format. The geometric model is sliced in accordance with the slices thickness parameters determined during the material

calibration process detailed previously. For all specimens manufactured in this investigation, the .stl format was utilized as the data input.

Preliminary design for tensile specimen

The preliminary design of the tensile specimen was tested to ascertain an optimal geometry capable of inducing rupture within the designated gauge length. Initiating with a ISO 527 Type 1BA specimen, which lacked a conductive trace, the specimen exhibited appropriate fracture behavior, thereby validating the design's effectiveness for further analysis.

Figure 3: view of broken specimen and image of surface fracture.

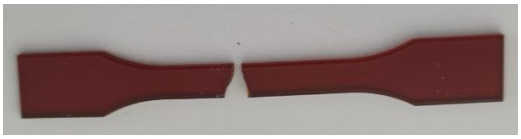

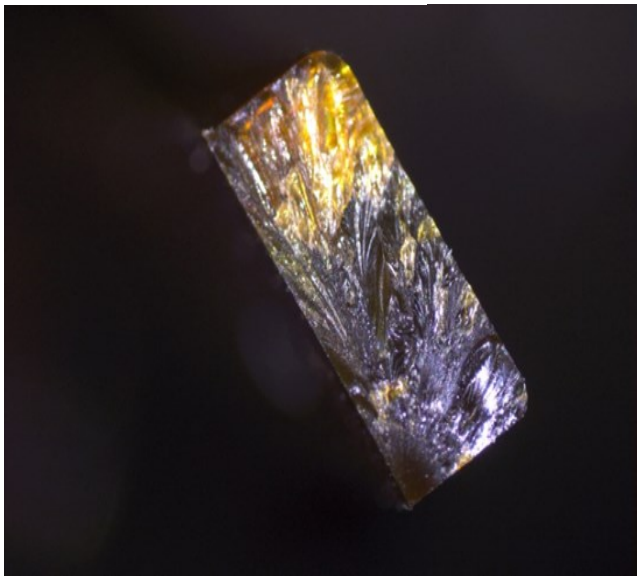

Source: figure by authors

Instead, the specimen exhibited fracture near the soldering pad as a result of the co-printed conductive trace.

An extensive examination of the ISO 527 specimen was performed, emphasizing critical parameters including the large radius to width ratio (W/w), the small radius to width ratio (r/w), and the stress concentration factor (Kt).

Type	s	w	W	L0	r	W/w	r/w	Kt	Fmax
ISO 527-2 1BA	2	5	10	25	30	2	6	1.65	580
ISO 527-2 5A	2	4	12.5	20	8	3.125	2	1.75	464
ISO 527-3 Type 5	1	6	25	25	14	4.166667	2.333333		348
ISO 527-2 1BA modified	2	3	10	25	22.3	3.333333	7.433333		348
ISO 527-2 5A modified	2	4	12.5	20	20.5	3.125	5.125		464
ISO 527-3 Type 5 modified	1	6	25	25	33.8	4.166667	5.633333		348
ISO 527-3 Type 1B	1	10	20	50	60	2	6	1.65	580
ISO 527-3 Type 4	1	25.4	38	50	22	1.496063	0.866142	1.55	1473.2
ISO 527-3 Type 2	1	10	10	50	0				580

The Type 5 specimen was selected for analysis; however, modifications were made to the dimensions of the small radius (r) and the large radius (W).

Additionally, a further analysis was conducted to evaluate the geometry of the soldering tab. The right geometry reported in Figure 4 was selected.

Figure 4: analyzed geometry for the soldering pads

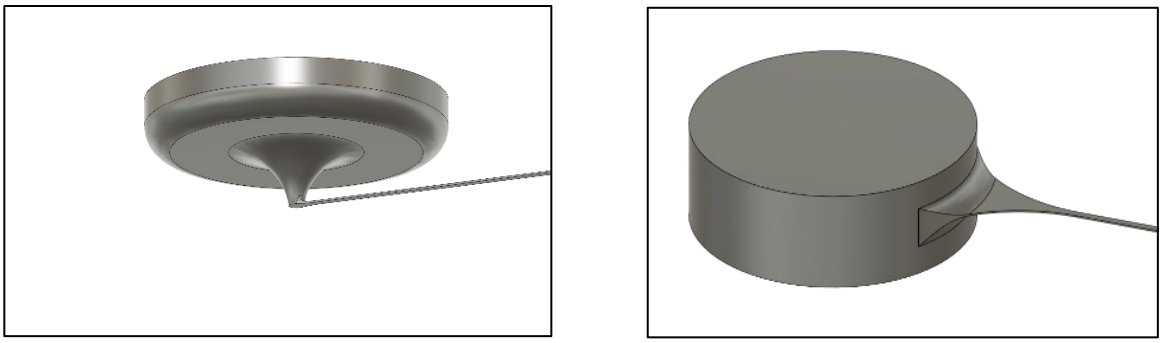

Source: figure by authors

The observations indicate that the specimen continues to exhibit fractures adjacent to the soldering pad. The soldering pad was ultimately relocated to an area with reduced stress concentrations, leading to the optimized and final design utilized for the tensile test.

Figure 5: rupture in different soldering pad positions.

Source: figure by authors

Position in printer plate

- 0°

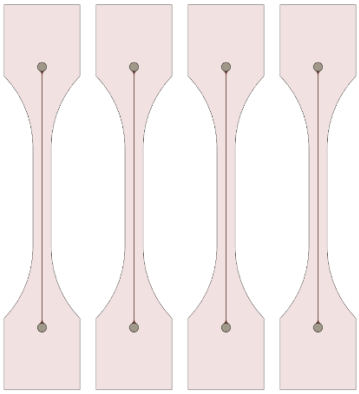

A B C D

- 45°

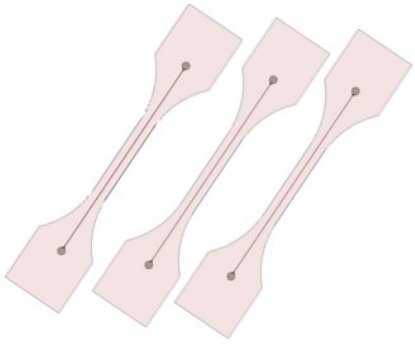

A B C

- 90°

A 

B 

C 

D 

Taguchi's DOE layout

The Design of Experiments (DOE) layout utilized for the analysis is summarized in Table. Each experimental run was replicated three times to ensure reliability and statistical robustness.

Run number	Printing parameters		
	A Trace width (µm)	B Trace thickness (µm)	C Printing direction (°)
1	72	10.75	0
2	72	17	45
3	72	34	90
4	144	10.75	45
5	144	17	90
6	144	34	0
7	288	10.75	90
8	288	17	0
9	288	34	45

Mechanical and electrical results of custom tensile test

			Mechanics			
RUN	Description	Sample	E1 (GPa)	ε_Yield(%)	σ_MAX (MPa)	Poisson
1	0.072_0.01075_0°	A	2.295	1.670	55.805	0.369
		B	2.262	1.812	56.812	0.368
		C	2.289	1.670	55.769	0.379
		D	2.300	1.652	57.067	0.369
2	0.072_0.017_45°	A	2.267	1.615	55.536	0.370
		B	2.278	1.619	56.240	0.370
		C	2.249	1.671	56.688	0.375
3	0.072_0.034_90°	A	2.299	1.613	55.408	0.353
		B	2.286	0.033	26.499	0.366
		C	2.320	1.625	57.331	0.370
		D	2.343	1.538	56.791	0.371
4	0.144_0.01075_45°	A	2.296	1.691	56.586	0.388
		B	2.291	1.604	56.173	0.360
		C	2.236	1.790	55.167	0.390

5	0.144_0.017_90°	A	2.265	1.740	58.226	0.377
		B	2.286	1.681	57.780	0.374
		C	2.304	1.630	55.200	0.382
		D	2.296	1.625	56.511	0.372
6	0.144_0.034_0°	A	2.328	1.626	57.440	0.376
		B	2.326	1.619	61.662	0.376
		C	2.316	1.629	56.921	0.374
		D	2.351	1.591	57.856	0.372
7	0.288_0.01075_90°	A	2.344	1.568	57.456	0.375
		B	2.307	1.540	58.894	0.373
		C	2.300	1.658	58.287	0.376
		D	2.284	1.647	57.347	0.375
8	0.288_0.017_0°	A	2.336	1.544	57.967	0.373
		B	2.316	1.635	58.855	0.375
		C	2.310	1.754	55.442	0.376
		D	2.308	1.708	57.342	0.374
9	0.288_0.034_45°	A	2.325	1.662	57.158	0.376
		B	2.279	1.721	53.326	0.368
		C	2.290	1.635	56.554	0.361

Table2: mechanical results of tensile test

			Electric						
RUN	**Description**	**Sample**	**(ΔR/R0)/ε**	**Degradation rate**	**ε_COS**	**ΔR_COS**	**ΔR_MAX**	**Conductivity 0**	**GF_COS**
1	0.072_0.01075_0°	A	0.012943	0.014	4.69505	0.059	0.060	2.917E+07	1.262
		B	0.013014	0.028	5.01735	0.067	0.075	2.826E+07	1.345
		C	0.012661	0.024	4.48104	0.058	0.059	2.936E+07	1.300
		D	0.013187	0.047	4.08497	0.058	0.104	2.917E+07	1.417
2	0.072_0.017_45°	A	0.012753	0.049	2.78256	0.036	0.210	3.144E+07	1.311
		B	0.012866	0.049	2.66540	0.035	0.240	3.142E+07	1.325
		C	0.012717	0.050	2.61440	0.034	0.393	3.138E+07	1.308
3	0.072_0.034_90°	A	0.012408	0.103	1.98870	0.025	1.113	3.500E+07	1.274
		B	-	-	-	-	-	-	-
		C	0.012559	0.091	1.79857	0.023	4.981	3.540E+07	1.291
		D	0.012293	0.097	1.83056	0.023	3.920	3.523E+07	1.266
4	0.144_0.01075_45°	A	0.011376	0.032	2.26584	0.027	0.160	2.844E+07	1.171
		B	0.012685	0.035	2.51649	0.033	0.125	2.840E+07	1.307
		C	0.011203	0.031	2.01974	0.023	0.112	2.852E+07	1.154
5	0.144_0.017_90°	A	0.012729	0.067	1.47431	0.019	2.615	3.050E+07	1.311
		B	0.012696	0.058	1.18514	0.015	1.119	3.048E+07	1.308
		C	0.011202	0.057	1.18547	0.014	0.561	3.064E+07	1.153

		D	0.012499	0.062	1.37656	0.018	0.981	3.061E+07	1.288
6	0.144_0.034_0°	A	0.011213	0.087	3.79173	0.044	0.561	2.608E+07	1.148
		B	0.011405	0.123	3.62831	0.042	3.247	2.558E+07	1.169
		C	0.011702	0.116	3.60480	0.043	1.103	2.546E+07	1.203
		D	0.011691	0.107	3.67565	0.044	2.384	2.576E+07	1.197
7	0.288_0.01075_90°	A	0.013542	0.055	1.22976	0.017	0.421	2.811E+07	1.394
		B	0.013164	0.052	1.12976	0.015	0.557	2.806E+07	1.354
		C	0.013799	0.052	1.19089	0.017	0.478	2.814E+07	1.421
		D	0.013375	0.055	1.24192	0.017	0.408	2.817E+07	1.377
8	0.288_0.017_0°	A	0.011587	0.060	4.74266	0.056	0.142	2.984E+07	1.190
		B	0.011672	0.062	4.53433	0.054	0.272	2.992E+07	1.201
		C	0.011814	0.018	4.36685	0.052	0.052	2.930E+07	1.189
		D	0.011678	0.063	4.30831	0.052	0.085	2.885E+07	1.201
9	0.288_0.034_45°	A	0.011180	0.514	2.87318	0.033	4.133	2.727E+07	1.149
		B	0.011360	0.693	2.85875	0.033	0.380	2.716E+07	1.167
		C	0.010990	0.501	2.83763	0.032	2.265	2.683E+07	1.132

Table3: electrical results of tensile test

ANOVA results

- **(ΔR/R0)/ε**

Regression Statistics	
Multiple R	0.86582397
R Square	0.74965115
Adjusted R Square	0.6745465
Standard Error	0.57048532
Observations	27

ANOVA

	gdl	*SQ*	*MQ*	*F*	*Significance F*
Regression	6	19.49093	3.248488	9.981420755	3.81075E-05
Residual	20	6.50907	0.325454		
Total	26	26			

- **ε_COS**

Regression Statistics	
Multiple R	0.98356505
R Square	0.96740021
Adjusted R Square	0.95762027
Standard Error	0.20586337
Observations	27

ANOVA

	gdl	*SQ*	*MQ*	*F*	*Significance F*
Regression	6	25.15241	4.192068	98.9168139	8.42E-14
Residual	20	0.847595	0.04238		

Total		26	26		

- **Degradetion rate**

Regression Statistics	
Multiple R	0.97902597
R Square	0.95849184
Adjusted R Square	0.94384191
Standard Error	0.22325225
Observations	24

ANOVA

	gdl	*SQ*	*MQ*	*F*	*Significance F*
Regression	6	19.56571	3.260952	65.42634559	8.3E-11
Residual	17	0.847307	0.049842		
Total	23	20.41302			

- **Conductivity**

Regression Statistics	
Multiple R	0.9780739
R Square	0.95662854
Adjusted R Square	0.94361711
Standard Error	0.23745082
Observations	27

ANOVA

	gdl	*SQ*	*MQ*	*F*	*Significance F*
Regression	6	24.87234	4.14539	73.5221303	1.43E-12
Residual	20	1.127658	0.056383		
Total	26	26			

Responce surface from predictive model

These are response variable related to the multilinear model reported in the article. In some cases, variability is observed, showing a trend different from the mean value presented. This occurs because the interpolation of the multilinear model is associated with an error (>20%), particularly in cases with small width and thickness values.

- **(ΔR/R0)/ε**

0°	**0.01075**	**0.01333**	**0.015917**	**0.0185**	**0.021083**	**0.023667**	**0.02625**	**0.028833**	**0.031417**	**0.034**
0.072	0.01278	0.01275	0.01272	0.01269	0.01266	0.01262	0.01259	0.01256	0.01253	0.01250
0.096	0.01269	0.01264	0.01259	0.01254	0.01249	0.01243	0.01238	0.01233	0.01228	0.01223
0.12	0.01261	0.01253	0.01246	0.01239	0.01232	0.01224	0.01217	0.01210	0.01203	0.01195
0.144	0.01252	0.01243	0.01233	0.01224	0.01215	0.01205	0.01196	0.01187	0.01177	0.01168
0.168	0.01244	0.01232	0.01221	0.01209	0.01198	0.01186	0.01175	0.01163	0.01152	0.01140
0.192	0.01235	0.01222	0.01208	0.01195	0.01181	0.01167	0.01154	0.01140	0.01127	0.01113
0.216	0.01227	0.01211	0.01195	0.01180	0.01164	0.01148	0.01133	0.01117	0.01101	0.01085

0.24	0.01218	0.01201	0.01183	0.01165	0.01147	0.01129	0.01111	0.01094	0.01076	0.01058
0.264	0.01210	0.01190	0.01170	0.01150	0.01130	0.01110	0.01090	0.01070	0.01050	0.01030
0.288	0.01201	0.01179	0.01157	0.01135	0.01113	0.01091	0.01069	0.01047	0.01025	0.01003

45°	**0.01075**	**0.01333**	**0.015917**	**0.0185**	**0.021083**	**0.023667**	**0.02625**	**0.028833**	**0.031417**	**0.034**
0.072	0.01305	0.01302	0.01299	0.01296	0.01293	0.01290	0.01287	0.01284	0.01281	0.01278
0.096	0.01296	0.01291	0.01286	0.01281	0.01276	0.01271	0.01266	0.01260	0.01255	0.01250
0.12	0.01288	0.01281	0.01273	0.01266	0.01259	0.01252	0.01244	0.01237	0.01230	0.01223
0.144	0.01280	0.01270	0.01261	0.01251	0.01242	0.01233	0.01223	0.01214	0.01205	0.01195
0.168	0.01271	0.01260	0.01248	0.01237	0.01225	0.01214	0.01202	0.01191	0.01179	0.01168
0.192	0.01263	0.01249	0.01235	0.01222	0.01208	0.01195	0.01181	0.01167	0.01154	0.01140
0.216	0.01254	0.01238	0.01223	0.01207	0.01191	0.01176	0.01160	0.01144	0.01128	0.01113
0.24	0.01246	0.01228	0.01210	0.01192	0.01174	0.01157	0.01139	0.01121	0.01103	0.01085
0.264	0.01237	0.01217	0.01197	0.01177	0.01157	0.01137	0.01118	0.01098	0.01078	0.01058
0.288	0.01229	0.01207	0.01185	0.01163	0.01141	0.01118	0.01096	0.01074	0.01052	0.01030

90°	**0.01075**	**0.01333**	**0.015917**	**0.0185**	**0.021083**	**0.023667**	**0.02625**	**0.028833**	**0.031417**	**0.034**
0.072	0.01332	0.01329	0.01326	0.01323	0.01320	0.01317	0.01314	0.01311	0.01308	0.01305
0.096	0.01324	0.01319	0.01313	0.01308	0.01303	0.01298	0.01293	0.01288	0.01283	0.01277
0.12	0.01315	0.01308	0.01301	0.01294	0.01286	0.01279	0.01272	0.01264	0.01257	0.01250
0.144	0.01307	0.01297	0.01288	0.01279	0.01269	0.01260	0.01251	0.01241	0.01232	0.01222
0.168	0.01298	0.01287	0.01275	0.01264	0.01252	0.01241	0.01229	0.01218	0.01206	0.01195
0.192	0.01290	0.01276	0.01263	0.01249	0.01235	0.01222	0.01208	0.01195	0.01181	0.01167
0.216	0.01281	0.01266	0.01250	0.01234	0.01219	0.01203	0.01187	0.01171	0.01156	0.01140
0.24	0.01273	0.01255	0.01237	0.01219	0.01202	0.01184	0.01166	0.01148	0.01130	0.01112
0.264	0.01265	0.01245	0.01225	0.01205	0.01185	0.01165	0.01145	0.01125	0.01105	0.01085
0.288	0.01256	0.01234	0.01212	0.01190	0.01168	0.01146	0.01124	0.01102	0.01080	0.01058

- **ε_COS**

0°	**0.01075**	**0.01333**	**0.015917**	**0.0185**	**0.021083**	**0.023667**	**0.02625**	**0.028833**	**0.031417**	**0.034**
0.072	4.608	4.508	4.409	4.309	4.209	4.110	4.010	3.911	3.811	3.711
0.096	4.625	4.521	4.417	4.314	4.210	4.106	4.002	3.898	3.794	3.690
0.12	4.643	4.534	4.426	4.318	4.210	4.102	3.994	3.885	3.777	3.669
0.144	4.660	4.547	4.435	4.323	4.210	4.098	3.985	3.873	3.761	3.648
0.168	4.677	4.560	4.444	4.327	4.210	4.094	3.977	3.860	3.744	3.627
0.192	4.694	4.573	4.452	4.332	4.211	4.090	3.969	3.848	3.727	3.606
0.216	4.712	4.586	4.461	4.336	4.211	4.086	3.960	3.835	3.710	3.585
0.24	4.729	4.599	4.470	4.340	4.211	4.082	3.952	3.823	3.693	3.564
0.264	4.746	4.612	4.479	4.345	4.211	4.078	3.944	3.810	3.677	3.543

0.288	4.763	4.625	4.487	4.349	4.211	4.074	3.936	3.798	3.660	3.522

45°	**0.01075**	**0.01333**	**0.015917**	**0.0185**	**0.021083**	**0.023667**	**0.02625**	**0.028833**	**0.031417**	**0.034**
0.072	3.169	3.069	2.970	2.870	2.771	2.671	2.571	2.472	2.372	2.272
0.096	3.186	3.082	2.979	2.875	2.771	2.667	2.563	2.459	2.355	2.251
0.12	3.204	3.095	2.987	2.879	2.771	2.663	2.555	2.447	2.338	2.230
0.144	3.221	3.108	2.996	2.884	2.771	2.659	2.546	2.434	2.322	2.209
0.168	3.238	3.121	3.005	2.888	2.771	2.655	2.538	2.421	2.305	2.188
0.192	3.255	3.134	3.013	2.893	2.772	2.651	2.530	2.409	2.288	2.167
0.216	3.273	3.147	3.022	2.897	2.772	2.647	2.522	2.396	2.271	2.146
0.24	3.290	3.160	3.031	2.902	2.772	2.643	2.513	2.384	2.254	2.125
0.264	3.307	3.173	3.040	2.906	2.772	2.639	2.505	2.371	2.238	2.104
0.288	3.324	3.186	3.048	2.910	2.773	2.635	2.497	2.359	2.221	2.083

90°	**0.01075**	**0.01333**	**0.015917**	**0.0185**	**0.021083**	**0.023667**	**0.02625**	**0.028833**	**0.031417**	**0.034**
0.072	1.730	1.630	1.531	1.431	1.332	1.232	1.132	1.033	0.933	0.833
0.096	1.747	1.643	1.540	1.436	1.332	1.228	1.124	1.020	0.916	0.812
0.12	1.765	1.656	1.548	1.440	1.332	1.224	1.116	1.008	0.899	0.791
0.144	1.782	1.669	1.557	1.445	1.332	1.220	1.107	0.995	0.883	0.770
0.168	1.799	1.682	1.566	1.449	1.332	1.216	1.099	0.982	0.866	0.749
0.192	1.816	1.695	1.575	1.454	1.333	1.212	1.091	0.970	0.849	0.728
0.216	1.834	1.708	1.583	1.458	1.333	1.208	1.083	0.957	0.832	0.707
0.24	1.851	1.721	1.592	1.463	1.333	1.204	1.074	0.945	0.815	0.686
0.264	1.868	1.734	1.601	1.467	1.333	1.200	1.066	0.932	0.799	0.665
0.288	1.885	1.747	1.609	1.471	1.334	1.196	1.058	0.920	0.782	0.644

- **Degradetion rate**

0°	**0.01075**	**0.01333**	**0.015917**	**0.0185**	**0.021083**	**0.023667**	**0.02625**	**0.028833**	**0.031417**	**0.034**
0.072	0.0498	0.0397	0.0296	0.0194	0.0093	-0.0008	-0.0109	-0.0210	-0.0311	-0.0412
0.096	0.0365	0.0339	0.0312	0.0285	0.0259	0.0232	0.0206	0.0179	0.0152	0.0126
0.12	0.0233	0.0281	0.0328	0.0376	0.0424	0.0472	0.0520	0.0568	0.0616	0.0664
0.144	0.0100	0.0222	0.0345	0.0467	0.0590	0.0712	0.0835	0.0957	0.1080	0.1202
0.168	-0.0033	0.0164	0.0361	0.0558	0.0755	0.0952	0.1149	0.1346	0.1543	0.1740
0.192	-0.0165	0.0106	0.0378	0.0649	0.0921	0.1192	0.1464	0.1735	0.2007	0.2278
0.216	-0.0298	0.0048	0.0394	0.0740	0.1086	0.1432	0.1778	0.2125	0.2471	0.2817
0.24	-0.0431	-0.0010	0.0411	0.0831	0.1252	0.1672	0.2093	0.2514	0.2934	0.3355
0.264	-0.0563	-0.0068	0.0427	0.0922	0.1417	0.1912	0.2408	0.2903	0.3398	0.3893
0.288	-0.0696	-0.0126	0.0443	0.1013	0.1583	0.2152	0.2722	0.3292	0.3862	0.4431

45°	0.01075	0.01333	0.015917	0.0185	0.021083	0.023667	0.02625	0.028833	0.031417	0.034
0.072	0.1010	0.0909	0.0808	0.0707	0.0606	0.0504	0.0403	0.0302	0.0201	0.0100
0.096	0.0877	0.0851	0.0824	0.0798	0.0771	0.0744	0.0718	0.0691	0.0665	0.0638
0.12	0.0745	0.0793	0.0841	0.0889	0.0937	0.0984	0.1032	0.1080	0.1128	0.1176
0.144	0.0612	0.0735	0.0857	0.0980	0.1102	0.1224	0.1347	0.1469	0.1592	0.1714
0.168	0.0479	0.0677	0.0874	0.1071	0.1268	0.1465	0.1662	0.1859	0.2056	0.2253
0.192	0.0347	0.0618	0.0890	0.1161	0.1433	0.1705	0.1976	0.2248	0.2519	0.2791
0.216	0.0214	0.0560	0.0906	0.1252	0.1598	0.1945	0.2291	0.2637	0.2983	0.3329
0.24	0.0082	0.0502	0.0923	0.1343	0.1764	0.2185	0.2605	0.3026	0.3446	0.3867
0.264	-0.0051	0.0444	0.0939	0.1434	0.1929	0.2425	0.2920	0.3415	0.3910	0.4405
0.288	-0.0184	0.0386	0.0956	0.1525	0.2095	0.2665	0.3234	0.3804	0.4374	0.4943

90°	0.01075	0.01333	0.015917	0.0185	0.021083	0.023667	0.02625	0.028833	0.031417	0.034
0.072	0.1522	0.1421	0.1320	0.1219	0.1118	0.1017	0.0915	0.0814	0.0713	0.0612
0.096	0.1390	0.1363	0.1336	0.1310	0.1283	0.1257	0.1230	0.1203	0.1177	0.1150
0.12	0.1257	0.1305	0.1353	0.1401	0.1449	0.1497	0.1545	0.1593	0.1640	0.1688
0.144	0.1124	0.1247	0.1369	0.1492	0.1614	0.1737	0.1859	0.1982	0.2104	0.2227
0.168	0.0992	0.1189	0.1386	0.1583	0.1780	0.1977	0.2174	0.2371	0.2568	0.2765
0.192	0.0859	0.1131	0.1402	0.1674	0.1945	0.2217	0.2488	0.2760	0.3031	0.3303
0.216	0.0726	0.1072	0.1419	0.1765	0.2111	0.2457	0.2803	0.3149	0.3495	0.3841
0.24	0.0594	0.1014	0.1435	0.1856	0.2276	0.2697	0.3117	0.3538	0.3959	0.4379
0.264	0.0461	0.0956	0.1451	0.1947	0.2442	0.2937	0.3432	0.3927	0.4422	0.4917
0.288	0.0328	0.0898	0.1468	0.2037	0.2607	0.3177	0.3747	0.4316	0.4886	0.5456

- **Conductivity**

0°	0.01075	0.01333	0.015917	0.0185	0.021083	0.023667	0.02625	0.028833	0.031417	0.034
0.072	2.85E+07	2.82E+07	2.80E+07	2.77E+07	2.74E+07	2.71E+07	2.68E+07	2.65E+07	2.63E+07	2.60E+07
0.096	2.87E+07	2.84E+07	2.80E+07	2.77E+07	2.74E+07	2.70E+07	2.67E+07	2.64E+07	2.60E+07	2.57E+07
0.12	2.89E+07	2.85E+07	2.81E+07	2.77E+07	2.73E+07	2.70E+07	2.66E+07	2.62E+07	2.58E+07	2.54E+07
0.144	2.90E+07	2.86E+07	2.82E+07	2.77E+07	2.73E+07	2.69E+07	2.64E+07	2.60E+07	2.56E+07	2.52E+07
0.168	2.92E+07	2.87E+07	2.82E+07	2.78E+07	2.73E+07	2.68E+07	2.63E+07	2.58E+07	2.54E+07	2.49E+07
0.192	2.94E+07	2.88E+07	2.83E+07	2.78E+07	2.73E+07	2.67E+07	2.62E+07	2.57E+07	2.51E+07	2.46E+07
0.216	2.96E+07	2.90E+07	2.84E+07	2.78E+07	2.72E+07	2.67E+07	2.61E+07	2.55E+07	2.49E+07	2.43E+07
0.24	2.97E+07	2.91E+07	2.85E+07	2.78E+07	2.72E+07	2.66E+07	2.60E+07	2.53E+07	2.47E+07	2.41E+07
0.264	2.99E+07	2.92E+07	2.85E+07	2.79E+07	2.72E+07	2.65E+07	2.58E+07	2.51E+07	2.45E+07	2.38E+07
0.288	3.01E+07	2.93E+07	2.86E+07	2.79E+07	2.72E+07	2.64E+07	2.57E+07	2.50E+07	2.42E+07	2.35E+07

45°	0.01075	0.01333	0.015917	0.0185	0.021083	0.023667	0.02625	0.028833	0.031417	0.034
0.072	2.99E+07	2.96E+07	2.93E+07	2.90E+07	2.88E+07	2.85E+07	2.82E+07	2.79E+07	2.76E+07	2.73E+07

0.096	3.01E+07	2.97E+07	2.94E+07	2.91E+07	2.87E+07	2.84E+07	2.81E+07	2.77E+07	2.74E+07	2.71E+07
0.12	3.02E+07	2.98E+07	2.95E+07	2.91E+07	2.87E+07	2.83E+07	2.79E+07	2.76E+07	2.72E+07	2.68E+07
0.144	3.04E+07	3.00E+07	2.95E+07	2.91E+07	2.87E+07	2.82E+07	2.78E+07	2.74E+07	2.69E+07	2.65E+07
0.168	3.06E+07	3.01E+07	2.96E+07	2.91E+07	2.86E+07	2.82E+07	2.77E+07	2.72E+07	2.67E+07	2.62E+07
0.192	3.07E+07	3.02E+07	2.97E+07	2.92E+07	2.86E+07	2.81E+07	2.76E+07	2.70E+07	2.65E+07	2.60E+07
0.216	3.09E+07	3.03E+07	2.98E+07	2.92E+07	2.86E+07	2.80E+07	2.74E+07	2.69E+07	2.63E+07	2.57E+07
0.24	3.11E+07	3.05E+07	2.98E+07	2.92E+07	2.86E+07	2.79E+07	2.73E+07	2.67E+07	2.61E+07	2.54E+07
0.264	3.13E+07	3.06E+07	2.99E+07	2.92E+07	2.85E+07	2.79E+07	2.72E+07	2.65E+07	2.58E+07	2.52E+07
0.288	3.14E+07	3.07E+07	3.00E+07	2.92E+07	2.85E+07	2.78E+07	2.71E+07	2.63E+07	2.56E+07	2.49E+07

90°	**0.01075**	**0.01333**	**0.015917**	**0.0185**	**0.021083**	**0.023667**	**0.02625**	**0.028833**	**0.031417**	**0.034**
0.072	3.13E+07	3.10E+07	3.07E+07	3.04E+07	3.01E+07	2.98E+07	2.95E+07	2.93E+07	2.90E+07	2.87E+07
0.096	3.14E+07	3.11E+07	3.08E+07	3.04E+07	3.01E+07	2.98E+07	2.94E+07	2.91E+07	2.88E+07	2.84E+07
0.12	3.16E+07	3.12E+07	3.08E+07	3.04E+07	3.01E+07	2.97E+07	2.93E+07	2.89E+07	2.85E+07	2.82E+07
0.144	3.18E+07	3.13E+07	3.09E+07	3.05E+07	3.00E+07	2.96E+07	2.92E+07	2.87E+07	2.83E+07	2.79E+07
0.168	3.19E+07	3.15E+07	3.10E+07	3.05E+07	3.00E+07	2.95E+07	2.91E+07	2.86E+07	2.81E+07	2.76E+07
0.192	3.21E+07	3.16E+07	3.10E+07	3.05E+07	3.00E+07	2.95E+07	2.89E+07	2.84E+07	2.79E+07	2.73E+07
0.216	3.23E+07	3.17E+07	3.11E+07	3.05E+07	3.00E+07	2.94E+07	2.88E+07	2.82E+07	2.76E+07	2.71E+07
0.24	3.25E+07	3.18E+07	3.12E+07	3.06E+07	2.99E+07	2.93E+07	2.87E+07	2.81E+07	2.74E+07	2.68E+07
0.264	3.26E+07	3.19E+07	3.13E+07	3.06E+07	2.99E+07	2.92E+07	2.86E+07	2.79E+07	2.72E+07	2.65E+07
0.288	3.28E+07	3.21E+07	3.13E+07	3.06E+07	2.99E+07	2.92E+07	2.84E+07	2.77E+07	2.70E+07	2.63E+07

Micrograph analysis for all the runs

- Run 1 C

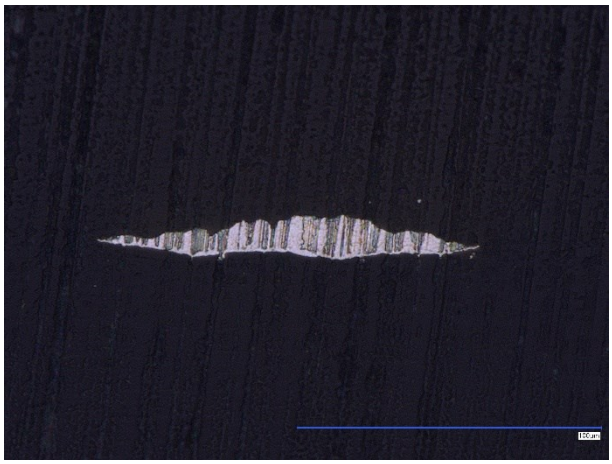

- Run 2 B

- Run 3 D
- Run 4 C

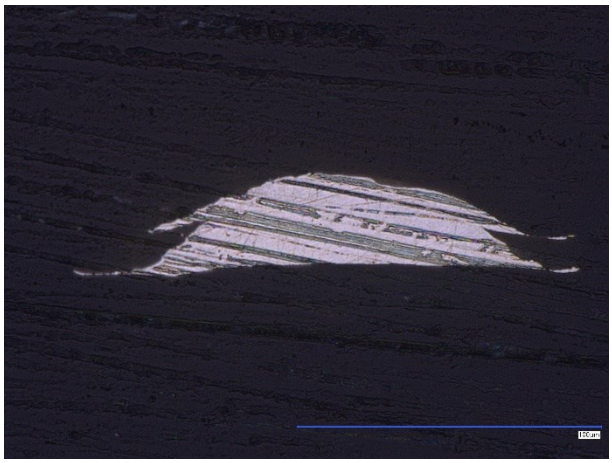

- Run 5 A

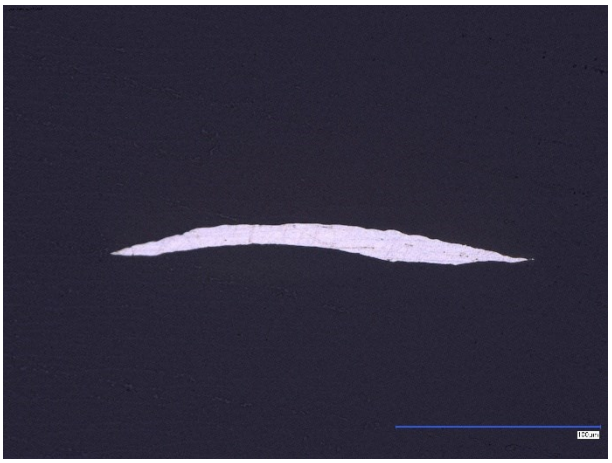

- Run 6 B

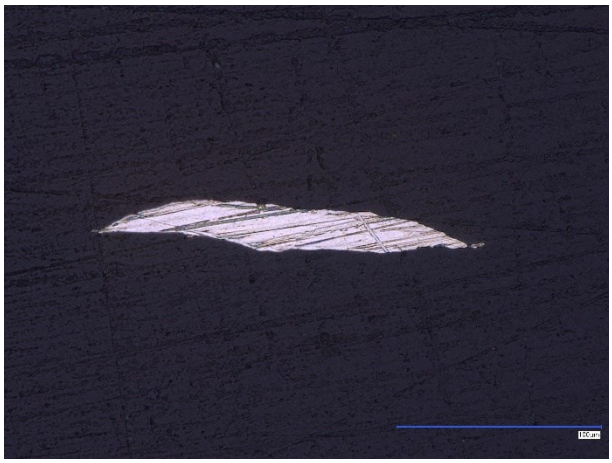

- Run 7 D

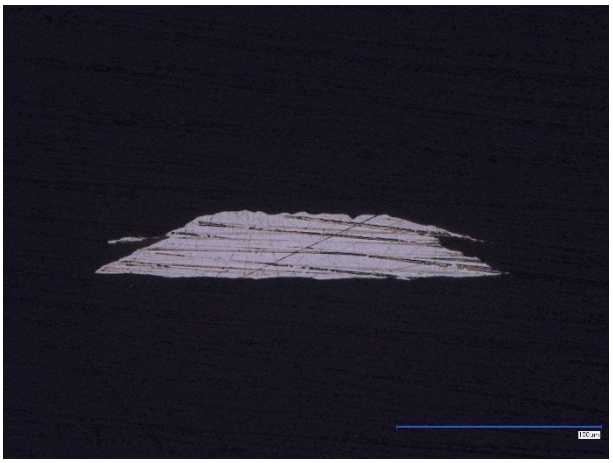

- Run 8 B

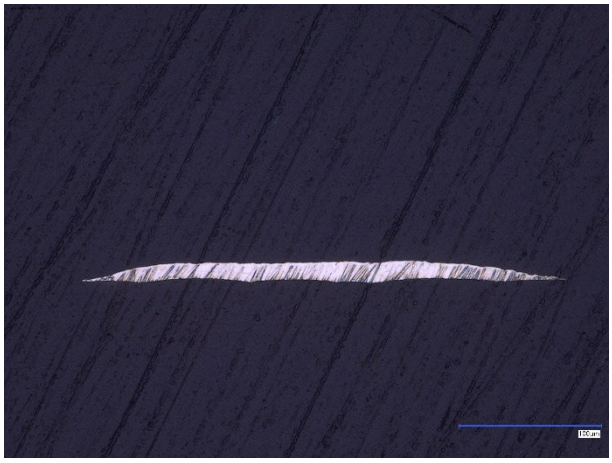

- Run 9 B

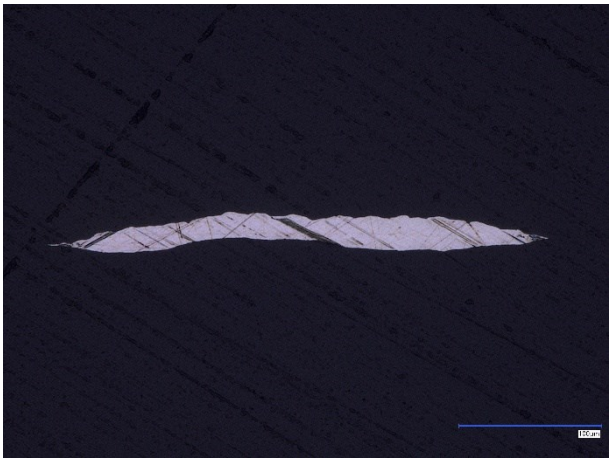

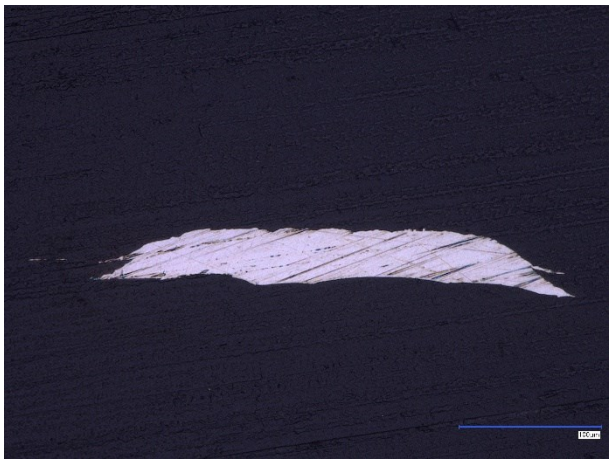

Printing error consideration

As reported in the literature by Li et al. [2], the average error primarily associated with thickness values reached a maximum of 20%. Similarly, in our post-test specimens, analyzed through micrographs, an error ranging from 0.5% to 20% was observed.

Based on these findings, and as suggested by Mueller et al. [4], who examined the final geometry and printing precision as functions of print bed position, orientation, and other factors, it can be argued that the DOE factors significantly influenced the precision of the printed specimens.

Run	Design section of CI (mm^2)	Mesured section of CI (mm^2)	ERROR (%)
1C	0.00080625	0.00081	0.462962963
2B	0.001275	0.001407847	9.436181631
3D	0.00255	0.002721101	6.287932715
4C	0.001548	0.001912119	19.0426871
5A	0.002448	0.002686495	8.87755235
6B	0.004896	0.004617319	6.03555873
7D	0.003096	0.003177891	2.576897697
8B	0.004896	0.005343856	8.380764751
9B	0.009792	0.009602228	1.976332993

Moreover, there are significant impacts on the overall dimensions of the specimen, particularly concerning total thickness.

RUN	Sample	Mean width	Mean thickness	Err % thickness	Days before calibration
1	A	5.980	1.005	-0.500	0
	B	6.003	1.003	-0.300	
	C	5.987	1.003	-0.300	
	D	5.953	1.001	-0.067	
2	A	6.023	0.988	1.200	3
	B	6.003	0.988	1.200	
	C	6.027	0.989	1.133	
3	A	6.003	0.928	7.167	6
	B	6.007	0.932	6.767	
	C	5.987	0.933	6.700	

	D	5.970	0.936	6.367	
4	A	6.010	0.983	1.667	9
	B	5.960	0.984	1.600	
	C	6.010	0.983	1.667	
5	A	5.997	0.934	6.633	12
	B	5.963	0.932	6.800	
	C	5.990	0.937	6.300	
	D	6.017	0.938	6.233	
6	A	6.003	0.961	3.933	15
	B	5.987	0.956	4.367	
	C	5.973	0.963	3.733	
	D	5.967	0.958	4.200	
7	A	5.987	0.900	10.033	25
	B	5.983	0.905	9.500	
	C	5.977	0.910	9.033	
	D	5.987	0.909	9.100	
8	A	6.010	0.992	0.800	17
	B	6.017	0.988	1.167	
	C	5.997	0.992	0.800	
	D	5.993	0.987	1.300	
9	A	6.007	0.961	3.933	22
	B	6.023	0.964	3.600	
	C	6.027	0.966	3.400	

All specimens were tested on the same day, one month after the final printing process.

Bibliography

[1] Nguyen MD, Yin Z, Rey R Del, Iacopi F, Yang Y. Additive Manufacturing Materials and Processes for Passive Electronics in Wireless Communication. IEEE Transactions on Materials for Electron Devices 2024;1:97–105. https://doi.org/10.1109/TMAT.2024.3440889.

[2] Li M, Cai J, Deng L, Li X, Iacopi F, Yang Y. Additively manufactured conductive and dielectric 3D metasurfaces for independent manipulation of broadband orbital angular momentum. Mater Des 2025;249:113500. https://doi.org/10.1016/j.matdes.2024.113500.

[3] Zhang J, Ahmadi M, Fargas G, Perinka N, Reguera J, Lanceros-Méndez S, et al. Silver Nanoparticles for Conductive Inks: From Synthesis and Ink Formulation to Their Use in Printing Technologies. Metals (Basel) 2022;12:234. https://doi.org/10.3390/met12020234.

[4] Mueller J, Shea K, Daraio C. Mechanical properties of parts fabricated with inkjet 3D printing through efficient experimental design. Mater Des 2015;86:902–12. https://doi.org/10.1016/j.matdes.2015.07.129.